AIAA Guidance, Navigation, and Control Conference and Exhibit
21 - 24 August 2006, Keystone, Colorado

AIAA 2006-6337

Adaptive Control of Evolving Gossamer Structures

Bong-Jun Yang*, Anthony J. Calise †, James I. Craig ‡
School of Aerospace Engineering, Georgia Institute of Technology
Atlanta, GA 30332

Mark S. Whorton §
Guidance, Navigation, and Mission Analysis, NASA Marshall Space Flight Center
Huntsville, AL

A solar sail is an example of a gossamer structure that is proposed as an propulsion system for future space missions. Since it is a large scale flexible structure that requires a long time for its deployment, active control may be required to prevent it from deviating into a non-recoverable state. In this paper, we conceptually address control of an evolving flexible structure using a growing double pendulum model. Controlling an evolving system poses a major challenge to control design because it involves time-varying parameters, such as inertia and stiffness. By employing a neural network based adaptive control, we illustrate that the evolving double pendulum can be effectively regulated when fixed-gain controllers are deficient due to presence of time-varying parameters.

I. Introduction

Solar sails have been proposed as a cost effective source of space propulsion for a variety of future space exploration missions. Solar sails gain momentum from incident and reflected photons, and the continuous sunlight pressure provides sufficient propulsive energy for space missions that, otherwise, is only possible with a significant amount of propellant for conventional rocket systems.[1] Currently, solar sail technology is being developed by the In-Space Propulsion Technology Program, managed by NASA's Science Mission Directorate and implemented by the In-Space Propulsion Technology Office at Marshall. The program's objective is to develop in-space propulsion technologies that enable NASA space science missions by significantly reducing cost, mass and travel times.

In general, the momentum transferred by a single photon is extremely small, and solar sails need to span a very large area to capture and reflect photons to achieve a sufficient propulsive force. As a result, some useful missions are only possible by use of ultra-lightweight sail films, lightweight deployable booms, and miniature avionics hardware. This makes solar sail structures unique in their limitations on strength and stiffness.[2] From the perspective of maneuvering/steering, solar sails are large gossamer structures that tightly couple attitude and structural dynamics to achieve thrust vector control. The vehicle attitude determines the orientation of the reflective sail surface with respect to the sun and hence determines the direction of the resultant thrust vector. Structural dynamics may impact the thrust vector accuracy by inducing a jitter in the reflected solar radiation and hence affecting direction and magnitude of the thrust vector. In addition, the flexibility of the booms and sail membranes may limit or adversely affect the stability and performance of the attitude control system.

Depending on imposed assumptions regarding the flexibility of solar sails, various hardware designs and control algorithms have been proposed in the literature. In [3–5], various hardware configurations and corresponding attitude control systems are investigated in relation to mission trajectories and orbits, with

*Research Engineer II, jun.yang@ae.gatech.edu, AIAA member
†Professor, anthony.calise@ae.gatech.edu, AIAA Fellow
‡Professor, james.craig@ae.gatech.edu, Senior AIAA member
§Branch Chief, mark.whorton@nasa.gov, AIAA Associate Fellow

a main uncertainty being solar radiation pressure disturbance caused by an uncertain offset between center-of-mass and center-of-pressure. In those methods, the problem of flexibility is avoided by assuming that the slow maneuvering required for low-thrust propulsion of solar sails still makes a low bandwidth attitude control system look "fast" in relative time-scales.[2] In [6], a solar sail is modelled as a linear flexible 6 degree-of-freedom spacecraft and different attitude control techniques are compared in the presence of parametric uncertainties. Ref. [7] considers flexibility and its influence on control effectiveness using idealized two-dimensional models. A distributed parameter model for a flexible solar sail is idealized as a rotating central hub with two opposing flexible booms, and linear feedback torque control is applied at the central hub.

In our effort, we conceptually address the problem of flexibility from a perspective that is different from those in the literature. Prior to the commencement of a solar sail mission, the packaged sail must be deployed into its operational configuration. Maintaining stable attitude dynamics of the sailcraft/bus system will be a challenge due to the enormous increase in sailcraft inertia as the support structure and membranes deploy. Therefore, from the perspective of modelling , a simple system-level deployment dynamics for the whole sailcraft is developed in order to assess the deployment behavior for a range of normal and abnormal conditions in [8]. From the perspective of control system design, growing structures induce their own challenges due to time-varying parameters as well as those typical for fully developed flexible systems. In design for an appropriate control method, major challenges are associated with the uncertainties inherent in flexible solar sails because a comprehensive test for structural analysis is not possible in ground tests due to gravity on Earth. Even when the vacuum and thermal conditions of the space environment are well simulated, solar sail tests should employ a gravity-offload system to mitigate the effects of gravity.[9] Further uncertainties in the material properties, test conditions, and modelling errors make it extremely difficult to obtain accurate flexibility characteristics of a flexible solar sail. Therefore, it is highly desirable for a control system to be able to adapt and compensate for system uncertainties.

In this paper, neural network (NN)-based adaptive control is considered to address the flexibilities, both during and after deployment, in the presence of parametric and dynamic uncertainties for control of attitude of a solar sail by suppressing unwanted vibrations. In order to avoid excessive complexities related to the modelling of a deploying flexible solar sail, we consider a growing single boom that supports the solar sail membrane and further simplify it as a double pendulum. Two masses evolve into its final configuration, mimicking the growth of the supporting boom of the structure, and we address how NN-based control system adapts to those adversary uncertainties during and after deployment. For further simplicity, the central hub from which the sail boom emerges is assumed fixed.

A critical feature that distinguishes evolving systems from the systems considered in the literature is time-varying parameters. In case of the double pendulum model, lengths and stiffness of the links are time-varying as the inertia of the pendulum evolves. A conventional approach for this case is to schedule gains by introducing a scheduling parameter. However, in our study, the time growth rate for the link is assumed unknown, and there is no way to determine when and how to set gains for controllers. Moreover, the control effectiveness slowly diminishes as the inertia of the system increases, and leads to gradual degradation for a fixed-gain controller. These challenges suggest that an adaptive approach may be the only viable solution for the evolving double pendulum. However, conventional adaptive approaches[10,11] allow for only linearly parameterized uncertainties and therefore are not well suited for this application.

The adaptive method employed in this paper is essentially the same as the one in [12] with the only difference being the use of an arbitrary reference model for each subsystem as suggested in [13]. A NN is employed to approximately cancel the uncertainty. It is well established that a NN can approximate any continuous function to any desired accuracy on a bounded set,[14] and this has been one of the main reasons given for using a NN in adaptive control approaches.[15–17] In an output feedback setting, a method that uses a memory unit of input/output delays to approximate an uncertainty has been proposed[18] and shown to be effective in output feedback applications.[19–22] Following the methodology in [21, 23], we assume that a nominal controller is already designed independently for each pendulum to maintain its angular position during deployment without any knowledge of flexibility characteristics and couplings that exits between the pendulums. That is, two nominal controllers are designed in a decoupled manner in which each subsystem is assumed independent from each other to avoid the complexity in designing a single controller for the coupled system of dynamics. Since the nominal controllers are intended to control only the local dynamics, without communication with each other, the overall design is equivalent to the decentralized approach described in [12].

The paper is organized as follows. In Section II we present the equations of motion for an evolving double

pendulum. In Section III, following a discussion on the essential features of evolving systems, the method of the augmenting adaptive controller design is presented. In Section IV, simulation results are described that support the validity of the overall approach. Conclusions and future research directions are given in Section V.

II. System Dynamics

Consider a single evolving boom consisting of two segments depicted in Figure 1, which represents a boom being deployed from the central hub. The nodes n_1, n_2, and n_3 represent the connecting point between the central hub and the first segment, the connecting point between two segments, and the tip of the boom, respectively. The terms t_1 and t_2 are the instants when the first segment and the second segment are fully deployed and are generally unknown in case anomalies arise during deployment. With regard to the evolving

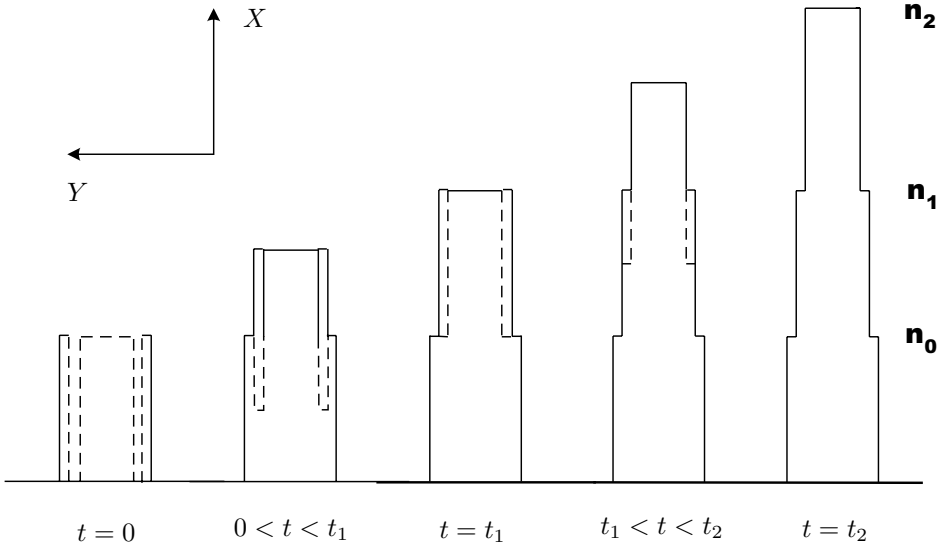

Figure 1. Time behavior for an evolving beam

dynamics in Figure 1, we assume the following:

- The segment of the boom continuously evolves.
- Sensors and actuators are collocated at nodes n_0 and n_1.
- The length of each segment is relatively short and treated as an rigid link.

Under the above assumptions, the system depicted in Figure 2 is considered as an analogy for the evolving boom for our study, in which the evolving pendulums represent varying inertia distribution. Figure 3 depicts possible sources for forces and torques in the configuration when the second pendulum in under deployment. The terms $K_1(t)$ and $K_2(t)$ are stiffness coefficients for torsional springs, which are introduced to model the flexibility of the boom. As seen in Figure 1, torsional stiffness is expected to depend on the length of the segment that is not deployed and therefore is modelled as time-varying parameters. The damping terms D_1 and D_2 are assumed constant. The terms $F_{a_i}(t)$ and $F_{b_i}(t)$ $(i = x, y)$ are external forces that are applied directly to the masses m_1 and m_2. The terms $u_1(t)$ and $u_2(t)$ are control torques provided by control systems. The effect of the sun light is detailed in the subsequent equation motion. Referring to Figures 2 and 3, the equation of motion for the evolving system is derived as follows.

A. When the first pendulum evolves ($0 \le t \le t_1$)

We assume that the pendulum length increases in a constant rate, and the length of the first pendulum is determined by

$$l_1(t) = l_{1_0} + \beta_l t, \tag{1}$$

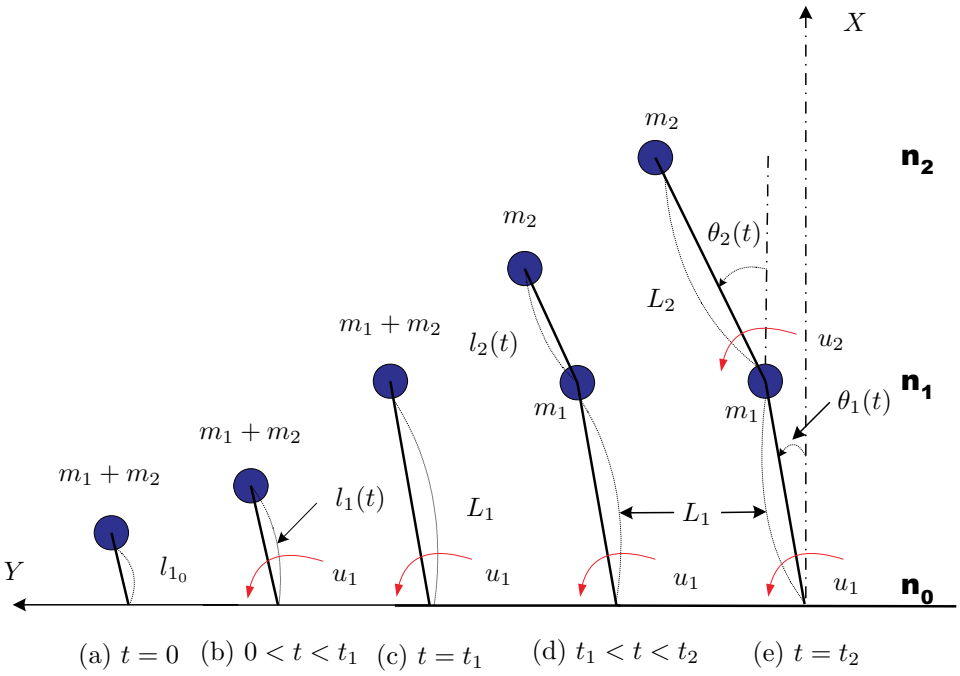

Figure 2. Time behavior for evolving pendulums

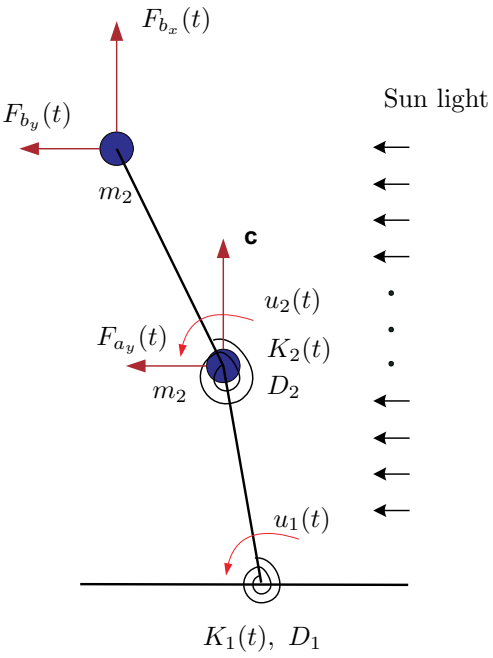

Figure 3. External forces while the second pendulum deploys

where l_{1_0} is the initial length for the mass m_1, and β_l is the increase rate for the pendulum. The stiffness, however, decreases as the pendulum evolves and is described by

$$K_1(t) = K_{1_0} - \alpha_{K_1} t, \tag{2}$$

where K_{1_0} is an initial stiffness constant, and α_{K_1} is the decrease rate for the stiffness. The resulting equation of motion is

$$\begin{aligned} &M_1(l_1(t),\theta_1)\ddot{\theta}_1 + D_1\dot{\theta}_1 + K_1(t)\theta_1 + f_{n_1}(l_1(t),\dot{\theta}_1,\theta_1) \\ &= u_1(t) + f_{d_1}(l_1(t),\theta_1) + f_{s_1}(l_1(t),\theta_1), \end{aligned} \tag{3}$$

where $M_1(l_1(t),\theta_1) = (m_1+m_2)l_1(t)^2$, D_1 is a damping coefficient, $f_{n_1}(l_1(t),\dot{\theta}_1),\theta_1)$ represents nonlinear terms due to Coriolis effect; $f_{n_1}(\dot{\theta}_1,\theta_1) = 2(m_1+m_2)l_1(t)\dot{l}_1\dot{\theta}_1 = 2(m_1+m_2)\beta_l l_1(t)\dot{\theta}_1$, $f_{d_1}(\theta_1) = -l_1(t)\sin\theta_1 F_{a_x}(t) + l_1(t)\cos\theta_1 F_{a_y}(t)$, and $F_{s_1}(l_1(t),\theta_1)$ is the torque caused by the solar pressure. Following Ref.[1], we model it as

$$f_{s_1}(l_1(t),\theta_1) = \frac{1}{2}\rho_s l_1(t)^2\cos\theta_1, \tag{4}$$

where ρ_s is the solar force applied at a unit length when the sunlight is perpendicular to the pendulum.

B. When the second pendulum evolves ($t_1 < t \le t_2$)

For this period, the first pendulum is fully deployed, i.e., $l_1(t) = l_{1_0} + \beta_l t_1 = L_1$, and $\dot{l}_1(t) = 0$. Similarly, $K_1(t) = K_{1_0} - \alpha_{K_1}t_1 = K_{1_f}$. However, the second pendulum is evolving, so we have

$$l_2(t) = l_{2_0} + \beta_l(t-t_1),\ K_2(t) = K_{2_0} - \alpha_{K_2}(t-t_1). \tag{5}$$

The equation of motion is then derived as

$$\begin{aligned} &M(l_2(t),\boldsymbol{\theta})\ddot{\boldsymbol{\theta}} + D\dot{\boldsymbol{\theta}} + K(t)\boldsymbol{\theta} + \boldsymbol{f}_n(l_2(t),\dot{\boldsymbol{\theta}},\boldsymbol{\theta}) \\ &= B_u\boldsymbol{u} + \boldsymbol{f}_s(l_2(t),\boldsymbol{\theta}) + B_a(\theta_1)\boldsymbol{F}_a + B_b(l_2(t),\boldsymbol{\theta})\boldsymbol{F}_b, \end{aligned} \tag{6}$$

where

$$\boldsymbol{\theta} = \begin{bmatrix} \theta_1 \\ \theta_2 \end{bmatrix},\ \boldsymbol{u} = \begin{bmatrix} u_1 \\ u_2 \end{bmatrix},\ \boldsymbol{F}_a = \begin{bmatrix} F_{a_x} \\ F_{a_y} \end{bmatrix},\ \boldsymbol{F}_b = \begin{bmatrix} F_{b_x} \\ F_{b_y} \end{bmatrix},$$

and

$$M(l_2(t),\boldsymbol{\theta}) = \begin{bmatrix} (m_1+m_2)L_1^2 & m_2L_1l_2(t)\cos(\theta_2-\theta_1) \\ m_2L_1l_2(t)\cos(\theta_2-\theta_1) & m_2l_2(t)^2 \end{bmatrix}, D = \begin{bmatrix} D_1+D_2 & -D_2 \\ -D_2 & D_2 \end{bmatrix},$$

$$K(t) = \begin{bmatrix} K_{1_f}+K_2(t) & -K_2(t) \\ -K_2(t) & K_2(t) \end{bmatrix}, B_u = \begin{bmatrix} 1 & 0 \\ 0 & 1 \end{bmatrix}, B_a(\theta_1) = \begin{bmatrix} -L_1\sin\theta_1 & L_1\cos\theta_1 \\ 0 & 0 \end{bmatrix},$$

$$B_b(l_2(t),\boldsymbol{\theta}) = \begin{bmatrix} -L_1\sin\theta_1 & L_1\cos\theta_1 \\ -l_2(t)\sin\theta_2 & l_2(t)\cos\theta_2 \end{bmatrix}. \tag{7}$$

The term $\boldsymbol{f}_n(l_2(t),\dot{\boldsymbol{\theta}},\boldsymbol{\theta})$ are due to Coriolis effects and centrifugal terms and are given by

$$\boldsymbol{f}_n(l_2(t),\dot{\boldsymbol{\theta}},\boldsymbol{\theta}) = \begin{bmatrix} 2m_2L_1\dot{l}_2(t)\dot{\theta}_2\cos(\theta_2-\theta_1) - m_2L_1l_2(t)\dot{\theta}_2^2\sin(\theta_2-\theta_1) \\ 2m_2l_2(t)\dot{l}_2(t)\dot{\theta}_2 + m_2L_1l_2(t)\dot{\theta}_1^2\sin(\theta_2-\theta_1) \end{bmatrix}, \tag{8}$$

and the solar torque $\boldsymbol{f}_s(l_2(t),\boldsymbol{\theta})$ is given by

$$\boldsymbol{f}_s(l_2(t),\boldsymbol{\theta}) = \begin{bmatrix} \frac{1}{2}\rho_sL_1^2\cos\theta_1 + \rho_sL_1l_2(t)\cos\theta_2\cos(\theta_2-\theta_1) \\ \frac{1}{2}\rho_sl_2(t)^2\cos\theta_2 \end{bmatrix}. \tag{9}$$

At the beginning of evolution, the second pendulum has the same angle as the first pendulum because they move together for $0 < t < t_1$, and the initial conditions for the second pendulum are set as $\theta_2(t_1) = \theta_1(t_1)$ and $\dot{\theta}_2(t_1) = \dot{\theta}_1(t_1)$.

C. After full deployment ($t > t_2$)

After the pendulums are fully deployed, $l_2(t) = l_{2_0} + \beta_l(t_2 - t_1) = L_2$ and $K_2 = K_{2_0} - \alpha_{K_2}(t_2 - t_1) = K_{2_f}$. This leads to

$$\begin{aligned} &M(\boldsymbol{\theta})\ddot{\boldsymbol{\theta}} + D\dot{\boldsymbol{\theta}} + K\boldsymbol{\theta} + \boldsymbol{f}_n(\dot{\boldsymbol{\theta}}, \boldsymbol{\theta}) \\ &= B_u\boldsymbol{u} + \boldsymbol{f}_s(\boldsymbol{\theta}) + B_a(\theta_1)\boldsymbol{F}_a + B_b(\boldsymbol{\theta})\boldsymbol{F}_b, \end{aligned} \tag{10}$$

where each terms are determined from (7)-(9) by letting $\dot{l}_2(t) = 0$ and $l_2(t) = L_2$. Note that after the full deployment, the lengths of both pendulums and torsional stiffness terms are constants and $l_2(t)$ term is removed in (10).

The parameters used in simulating the evolving beams are

$$\begin{aligned} &m_1 = m_2 = 2\ (m),\ l_{1_0} = l_{2_0} = 1\ (m),\ L_1 = L_2 = 10\ (m),\ t_1 = 50sec.,\ t_2 = 100sec.,\ \beta_l = \frac{L_1 - l_{1_0}}{t_1}(m/s), \\ &K_{1_0} = K_{2_0} = 2\ (N/m),\ K_{1_f} = K_{2_f} = 0.5\ (N/m),\ \alpha_{K_1} = \alpha_{K_2} = \frac{K_{1_0} - K_{1_f}}{t_1}\ (N/s), \\ &D_1 = 0.0001(N \cdot s/m),\ D_2 = 0.0008\ (N \cdot s/m),\ \rho_s = 0.01\ (N/m). \end{aligned} \tag{11}$$

The initial conditions are set as $\theta_1(0) = 20^o$, $\dot{\theta}_1(0) = 0$.

III. Control Design

A. Control objective and decentralized architecture

In the deploying double pendulum in Figure 2, the control system is also assumed to evolve and is immediately activated when each pendulum starts to evolve. The measurements are angular displacements for each pendulums, i.e., $y_1(t) = \theta_1(t)$ for $0 < t \leq t_1$, and $y_1(t) = \theta_1(t),\ y_2(t) = \theta_2(t)$ for $t > t_1$, and $u_1(t)$ and $u_2(t)$ are control torques and are available at the same time when the measurements are available. The control objective is to design a control law for u_1 for $0 < t \leq t_1$ and u_1 and u_2 for $t > t_2$ so as to stabilize the pendulum during and after deployment when the deployment rate (therefore, the length of the pendulum during deployment) is not available, which mimics the situation in which proper positioning of the solar sail system is impeded due to anomalies in deploying process.

This objective poses serious challenges in designing a control law for u_1 and u_2. First, system parameters are slowly time-varying with its rate proportional to the unknown rate of evolution. Second, the control effectiveness lessens, as the system evolves, and hence leads to gradual degradation of system performance for a fixed-gain controller. These challenges makes an adaptive approach be a viable solution, and we seek to control the deploying dynamics using the method in [13,23,24] that is formulated in a way that augments an fixed-gain linear controller by adding adaptive control. We assume that a lead controller is already designed for each pendulum to maintain its angular position during deployment. They are designed in a decoupled manner, in which θ_1 and θ_2 dynamics are assumed independent from each other, without considering flexibility. In the sense that θ_1 controller and θ_2 controller are in independent control of dynamics without any communication each other, the overall design architecture falls into the decentralized one described in [12]. When we augment the lead controllers using NNs, we also introduce an arbitrary reference model as in [13].

Figure 4 lays out the control architecture for the evolving pendulum system. In Figure 4(a), the second control system is only active for $t > t_2$ and denoted in blue double dotted line. The θ_1 and θ_2 controllers have the same architecture, and Figure 4(b) shows how the θ_1-controller is designed. The block representing the adaptive portion of the design is shaded. Note that applying the same reference command θ_c for both controllers means that the objective of two controllers is to synchronize their motion.

B. Design of a fixed-gain controller $G_{ec}(s)$

The linear controller is designed considering the following models for m_1 and m_2

$$\begin{aligned} &\ddot{\theta}_1 = b_1 u_1,\ t > 0 \\ &\ddot{\theta}_2 = b_2 u_2,\ t > t_1. \end{aligned} \tag{12}$$

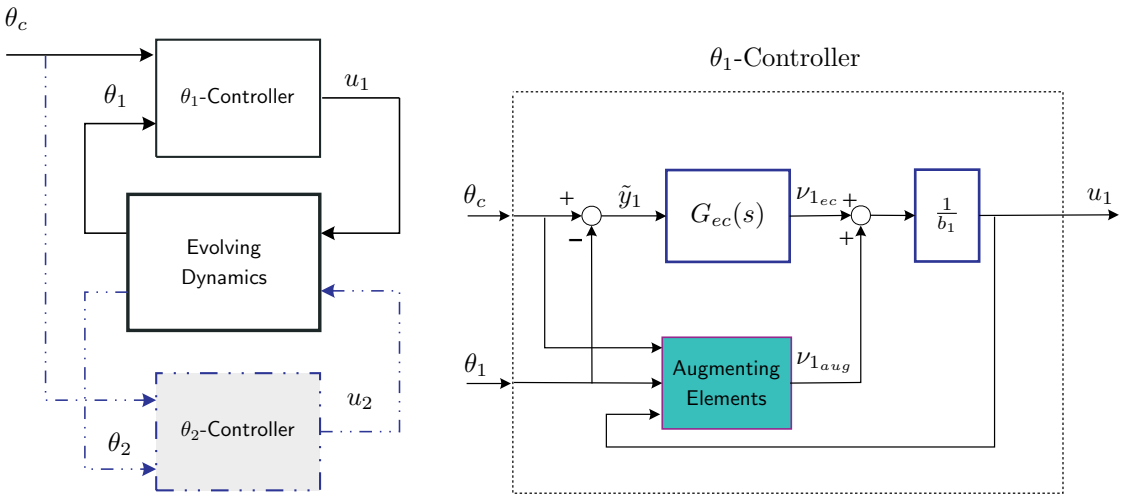

(a) Overall Control Architecture

(b) Inside of θ_1-Controller

Figure 4. Control System Architecture

The control effectiveness terms are defined as

$$b_1 = \frac{1}{(\hat{m}_1 + \hat{m}_2) l_{1_0}^2}, \; b_2 = \frac{1}{\hat{m}_2 l_{2_0}^2}, \tag{13}$$

where $\hat{m}_1 = 1$ and $\hat{m}_2 = 1$ are estimates for m_1 and m_2. Note that the plant model does not consider any flexibility or coupling dynamical effects between two pendulums. Letting

$$u_1 = \frac{1}{b_1}\nu_1, \; u_2 = \frac{1}{b_2}\nu_2 \tag{14}$$

leads to

$$\ddot{\theta}_i = \nu_i, \; i = 1, 2. \tag{15}$$

For $G_{ec}(s)$ in Figure 4(b), a lead compensator is designed

$$\nu_{i_{ec}} = G_{ec}(s)\tilde{y}_i = K_p \tilde{y}_i + K_d \frac{s}{s/\omega_l + 1}\tilde{y}_i, \tag{16}$$

where $\tilde{y}_i = \theta_c - \theta_i$ $(i = 1, 2)$, and $K_p = 0.0163$ $K_d = 3.1442$, and $\omega_l = 20$(rad/s) leads to the closed-loop poles of $-18.8904, -1.1044, -0.0052$ for the systems in (12).

With (14), compared to the plant model in (15), the true system in (3) ,(6), and (10) is described by

$$\begin{aligned} \ddot{\theta}_1 &= \nu_1 + \Delta_1(t), \; t > 0 \\ \ddot{\theta}_2 &= \nu_2 + \Delta_2(t), \; t > t_1, \end{aligned} \tag{17}$$

where the modelling error $\Delta_i(t)$ $(i = 1, 2)$ are defined as follows.

- For $0 < t \leq t_1$

$$\begin{aligned} \Delta_1(t) =& \frac{1}{M(l_1(t), \theta_1)} \left[-D_1\dot{\theta}_1 - K_1\theta_1 - f_n(l_1(t), \dot{\theta}_1, \theta_1) + f_{s_1}(l_1(t), \theta_1) + f_d(l_1(t), \theta_1) \right] \\ &+ b_1 \left(\frac{(\hat{m}_1 + \hat{m}_2) l_{1_0}^2}{(m_1 + m_2) l_1(t)^2} - 1 \right) u_1, \end{aligned} \tag{18}$$

  where the control effectiveness term is explicitly given to show its time-varying nature due to increase in the inertia. It is bounded according to the following inequalities

$$b_1 \left(\frac{(\hat{m}_1 + \hat{m}_2)}{(m_1 + m_2)} - 1 \right) > b_1 \left(\frac{(\hat{m}_1 + \hat{m}_2) l_{1_0}^2}{(m_1 + m_2) l_1(t)^2} - 1 \right) < b_1 \left(\frac{(\hat{m}_1 + \hat{m}_2) l_{1_0}^2}{(m_1 + m_2) L_1^2} - 1 \right) > -b_1$$

The choice of b_1 in (12) guarantees that

$$|b_1 u_1| > \left| b_1 \left(1 - \frac{(\hat{m}_1 + \hat{m}_2) l_{1_0}^2}{(m_1 + m_2) l_1(t)^2} \right) u_1 \right|$$

whenever $u_1 \neq 0$. The first term in (18) tends to decrease, with $\dot{\theta}_1$ and θ_1 fixed, as m_1 evolves except the solar force term

$$\frac{f_{s_1}(l_1(t), \theta_1)}{M(l_1(t), \theta_1)} = \frac{\rho_s \cos\theta_1}{2(m_1 + m_2)}$$

because the inertia term $M(l_1(t), \theta_1)$ is of the second order with respect to the pendulum length $l_1(t)$.

- For $t_1 < t \leq t_2$

  Letting $\boldsymbol{\Delta}(t) = [\Delta_1(t),\ \Delta_2(t)]^\top$, similarly as in (18), we have

$$\begin{aligned} \boldsymbol{\Delta}(t) =& M(l_2(t), \boldsymbol{\theta})^{-1} \Big[-D\dot{\boldsymbol{\theta}} - K(t)\boldsymbol{\theta} - \boldsymbol{f}_n(l_2(t), \dot{\boldsymbol{\theta}}, \boldsymbol{\theta}) + \boldsymbol{f}_s(l_2(t), \boldsymbol{\theta}) \\ & + B_a(\theta_1)\boldsymbol{F}_a + B_b(l_2(t), \boldsymbol{\theta})\boldsymbol{F}_b \Big] + \underbrace{\left(M(l_2(t), \boldsymbol{\theta})^{-1} B_u - \hat{B} \right)}_{B_\delta} \boldsymbol{u}, \end{aligned} \tag{19}$$

  where $\hat{B} = \text{diag}\{b_1,\ b_2\}$. The expression for the control effectiveness term is

$$B_\delta = \begin{bmatrix} b_1 \left(\frac{(\hat{m}_1 + \hat{m}_2) l_{1_0}^2}{(m_1 + m_2) L_1^2} \frac{1}{1 - \frac{m_2}{m_1 + m_2} \cos^2(\theta_2 - \theta_1)} - 1 \right) & -\frac{1}{(m_1 + m_2) L_1^2} \frac{L_1 / l_2(t) \cos(\theta_2 - \theta_1)}{1 - \frac{m_2}{m_1 + m_2} \cos^2(\theta_2 - \theta_1)} \\ -\frac{1}{(m_1 + m_2) L_1^2} \frac{L_1 / l_2(t) \cos(\theta_2 - \theta_1)}{1 - \frac{m_2}{m_1 + m_2} \cos^2(\theta_2 - \theta_1)} & b_2 \left(\frac{\hat{m}_2 l_{2_0}^2}{m_2 l_2(t)^2} \frac{1}{1 - \frac{m_2}{m_1 + m_2} \cos^2(\theta_2 - \theta_1)} - 1 \right) \end{bmatrix}.$$

- For $t > t_2$

$$\begin{aligned} \boldsymbol{\Delta}(t) = \boldsymbol{\Delta}(\dot{\boldsymbol{\theta}}, \boldsymbol{\theta}) =& M(\boldsymbol{\theta})^{-1} \Big[-D\dot{\boldsymbol{\theta}} - K\boldsymbol{\theta} - \boldsymbol{f}_n(\dot{\boldsymbol{\theta}}, \boldsymbol{\theta}) + \boldsymbol{f}_s(\boldsymbol{\theta}) \\ & + B_a(\theta_1)\boldsymbol{F}_a + B_b(\boldsymbol{\theta})\boldsymbol{F}_b \Big] + \left(M(\boldsymbol{\theta})^{-1} B_u - \hat{B} \right) \boldsymbol{u}. \end{aligned} \tag{20}$$

C. Augmenting elements

The augmenting approaches in [23, 24] define a reference model, which determines the best possible performance, which is made up of the plant regulated by the existing control system. This leads to having a reference model whose order equals the order of the plant model plus the order of the controller. For complex systems, this can be excessively high. As an alternative, we can employ an arbitrarily chosen reference model that has the same relative degree of the plant.[13]

Following the rationale in [13], we introduce a second order reference model described by

$$\ddot{\theta}_r = -2\zeta_r \omega_r \dot{\theta}_r + \omega_r^2 \theta_r + \omega_r^2 \theta_c, \tag{21}$$

where $\zeta_r = 0.9$, $\omega_r = 1$ (rad/s), for both θ_1 and θ_2 dynamics. Since the augmenting elements in Figure 4(b) are exactly the same, we use the subscript i to denote both 1 and 2. As seen in Figure 4(b), let

$$\nu_i = \nu_{i_{ec}} + \nu_{i_{aug}}. \tag{22}$$

By defining the tracking error as

$$e_i = \theta_r - \theta_i, \tag{23}$$

comparing (17) to (21) leads to

$$\ddot{e}_i = \ddot{\theta}_r - \nu_{i_{aug}} + \Delta_i'(t), \tag{24}$$

where

$$\Delta_i'(t) = \Delta_i(t) - \nu_{i_{ec}}. \tag{25}$$

By letting

$$\nu_{i_{aug}} = \ddot{\theta}_r + \nu_{i_{dc}} - \nu_{i_{ad}}, \tag{26}$$

we have

$$\ddot{e}_i = -\nu_{i_{dc}} + \nu_{i_{ad}} - \Delta_i'(t), \tag{27}$$

which is exactly the same as the one in [25, 26] and hereafter we follow the design method in [25, 26]. The compensator $\nu_{i_{dc}}$ is designed to stabilize the dynamics in (27) when $\nu_{i_{ad}} - \Delta_i'(t) = 0$, and $\nu_{i_{ad}}$ is an adaptive signal that approximates for the uncertainty $\Delta_i'(t)$.

With the definition

$$\boldsymbol{e}_i = \begin{bmatrix} e_i & \dot{e}_i \end{bmatrix}^\top = \begin{bmatrix} e_{i_1} & \dot{e}_{i_2} \end{bmatrix}^\top, \tag{28}$$

the error dynamics in (27) can be written in the following state space form

$$\begin{aligned} \dot{\boldsymbol{e}}_i =& A\boldsymbol{e}_i + \boldsymbol{b}(-\nu_{i_{dc}} + \nu_{i_{ad}} - \Delta_i') \\ e_i =& \boldsymbol{c}^\top \boldsymbol{e}_i, \end{aligned} \tag{29}$$

where

$$A = \begin{bmatrix} 0 & 1 \\ 0 & 0 \end{bmatrix},\ \boldsymbol{b} = \begin{bmatrix} 0 \\ 1 \end{bmatrix},\ \boldsymbol{c}^\top = \begin{bmatrix} 1 \\ 0 \end{bmatrix}. \tag{30}$$

The compensator $\nu_{i_{dc}}$ is designed similarly as in (16)

$$\nu_{i_{dc}} = K_{dc_p} e_i + K_{dc_d} \hat{e}_{i_2}, \tag{31}$$

where $K_{dc_p} = 0.1$, $K_{dc_d} = 0.2$, and $\hat{e}_{i_2}$ is obtained by

$$\hat{e}_{i_2} = \frac{s}{s/\omega_l + 1} e_i. \tag{32}$$

The compensator is written in state space form as

$$\begin{aligned} \dot{x}_{dc} =& a_c x_{dc} + b_c e_i \\ \nu_{i_{dc}} =& c_c x_{dc} + d_c e_i, \end{aligned} \tag{33}$$

and results in the following closed-loop error dynamics

$$\dot{\boldsymbol{E}} = \bar{A}\boldsymbol{E} + \bar{\boldsymbol{b}}(\nu_{i_{ad}} - \Delta_i'), \tag{34}$$

whose poles are located at $-19.80, -0.10 \pm 0.3j$, and

$$\boldsymbol{E} = \begin{bmatrix} \boldsymbol{e}_i \\ x_{dc} \end{bmatrix},\ \bar{A} = \begin{bmatrix} A - \boldsymbol{b} d_c c_c & -\boldsymbol{b} c_c \\ b_c \boldsymbol{c}^\top & a_c \end{bmatrix},\ \bar{\boldsymbol{b}} = \begin{bmatrix} \boldsymbol{b} \\ 0 \end{bmatrix}. \tag{35}$$

Since $\bar{A}$ is Hurwitz, for any $Q > 0$, there exists a $P > 0$ such that

$$\bar{A}P + P\bar{A} + Q = 0. \tag{36}$$

In simulation Q is set as $I_{3\times 3}$.The adaptive signal $\nu_{i_{ad}}$ is implemented using a NN, and the overall augmenting elements are depicted in Figure 5.

D. Adaptive element

A single hidden-layer NN (SHLNN) is used to approximate $\Delta_i'(t)$ in (25) using a memory unit of sampled input/output pairs. With t fixed, there exist bounded constant weights, $W(t), V(t)$, such that:

$$\Delta_i'(t) = \boldsymbol{W}(t)^\top \boldsymbol{\sigma}(V(t)^\top \boldsymbol{\mu}) + \varepsilon(\boldsymbol{\mu}),\ |\varepsilon(\boldsymbol{\mu})| \leq \epsilon^*, \tag{37}$$

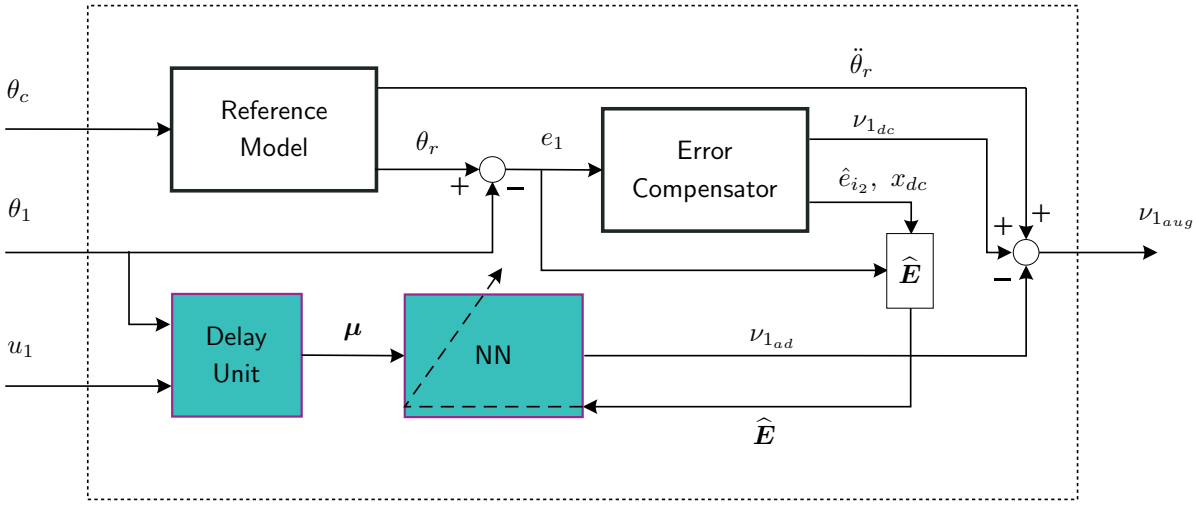

Figure 5. Diagram for augmenting elements

where $\varepsilon(\boldsymbol{\mu})$ is the NN reconstruction error, which is upper bounded by ϵ^* on a compact domain of interest, and $\boldsymbol{\mu}$ is the network input vector

$$\begin{aligned}\boldsymbol{\mu}(t) &= [\ 1 \quad \bar{\boldsymbol{u}}_d^T(t) \quad \bar{\boldsymbol{y}}_d^T(t)\ ]^T \\ \bar{\boldsymbol{u}}_d^T(t) &= [u_i(t) \quad u_i(t-d) \quad \cdots u_i(t-(n_1-r-1)d)]^T \\ \bar{\boldsymbol{y}}_d^T(t) &= [y_i(t) \quad y_i(t-d) \cdots y_i(t-(n_1-1)d)]^T\end{aligned} \tag{38}$$

in which n_1 is the length of the window and is generally required to be greater than or equal to the system dimension, $d > 0$ is a time-delay, r is the relative degree of the output, $\boldsymbol{\sigma}$ is a vector of squashing functions, $\sigma(\cdot)$, whose i^{th} element is defined as $\left[\boldsymbol{\sigma}(V^\top \boldsymbol{\mu})\right]_i = \sigma\left[(V^\top \boldsymbol{\mu})_i\right]$, and $y_i(t)$ is an output of the system, i.e., $y_i(t) = \theta_i(t)$. Notice that $W_i(t)$ and $V_i(t)$ are time-varying due to the time-varying parameters $l_i(t)$ and $K_i(t)$. We assume that the varying rate for those parameters is much more smaller than the bandwidth of the controller we design, and those parameters can be treated as constants for some time period $[t-\delta, t+\delta]$, $\delta > 0$. In other words, from the control design perspective, the ideal weights $\boldsymbol{W}(t)$ and $V(t)$ are assumed constants because they vary much more slowly than the NN weights. The squashing functions are chosen as sigmoidal functions

$$[\boldsymbol{\sigma}(V(t)^\top \boldsymbol{\mu})]_i = \frac{1}{1+e^{-a(V(t)^\top \boldsymbol{\mu})_i}},\ i = 1, \ldots, N, \tag{39}$$

where $a = 1$ represents the activation potential, and N is the number of neurons in the hidden layer.

The adaptive signal $\nu_{i_{ad}}$ is designed as

$$\nu_{i_{ad}} = \widehat{\boldsymbol{W}}(t)^\top \boldsymbol{\sigma}(\widehat{V}(t)^\top \boldsymbol{\eta}) \tag{40}$$

where $\widehat{\boldsymbol{W}}(t)$ and $\widehat{V}(t)$ are estimate weights for $W(t)$ and $V(t)$ and are adapted on-line. They are update by

$$\begin{aligned}\dot{\widehat{\boldsymbol{W}}} &= -\Gamma_W[(\hat{\boldsymbol{\sigma}} - \hat{\sigma}'\widehat{V}^\top \boldsymbol{\eta})\widehat{\boldsymbol{E}}^\top P\bar{\boldsymbol{b}} + k\widehat{\boldsymbol{W}}] \\ \dot{\widehat{V}} &= -\Gamma_V[\widehat{\boldsymbol{E}}^\top P\bar{\boldsymbol{b}}\boldsymbol{\mu}\widehat{\boldsymbol{W}}^\top \hat{\sigma}' + k\widehat{V}]\,,\end{aligned} \tag{41}$$

in which $\Gamma_W, \Gamma_V > 0$ are positive definite adaptation gain matrices, $k > 0$ is a $\sigma-$modification constant, $\hat{\boldsymbol{\sigma}} \triangleq \boldsymbol{\sigma}(\widehat{V}\boldsymbol{\eta})$, $\hat{\sigma}'$ is the Jacobian computed at the estimates, P is obtained from (36), and $\widehat{\boldsymbol{E}}$ is an estimate for $\boldsymbol{E}$ in (34) and is obtained from (29), (32), and (33)

$$\widehat{\boldsymbol{E}} = \begin{bmatrix} e_{i_1} & \hat{e}_{i_2} & x_{dc} \end{bmatrix}^\top, \tag{42}$$

instead of designing an observer as done in [26].

In simulation, two SHLNNs whose hidden layer consists of 5 neurons ($N = 5$) are employed for θ_1 and θ_2 dynamics. Since θ_i has the relative degree 2, 2 delayed values of u_i are used, together with 4 delayed values of θ_i to construct an input for each NN.[26] The delay $d = 0.1$, and the parameters for each NN are

$$\Gamma_W = 25I,\ \Gamma_V = 25I,\ k = 1, \tag{43}$$

where I is the identity matrix with compatible dimension.

IV. Simulation Results

Figure 6 shows how the structure of the evolving pendulum in Figure 2 changes as time evolves. When the first link ($1_1(t)$) finishes its expansion at $t = 50$ sec., the second link ($l_2(t)$) starts to expand and stops its deployment at $t = 100$ sec., where the whole system forms into its final configuration as shown in Figure 6(a). Figure 6(b) indicates that during deployment, the stiffness of each link declines from 2 to 0.5.

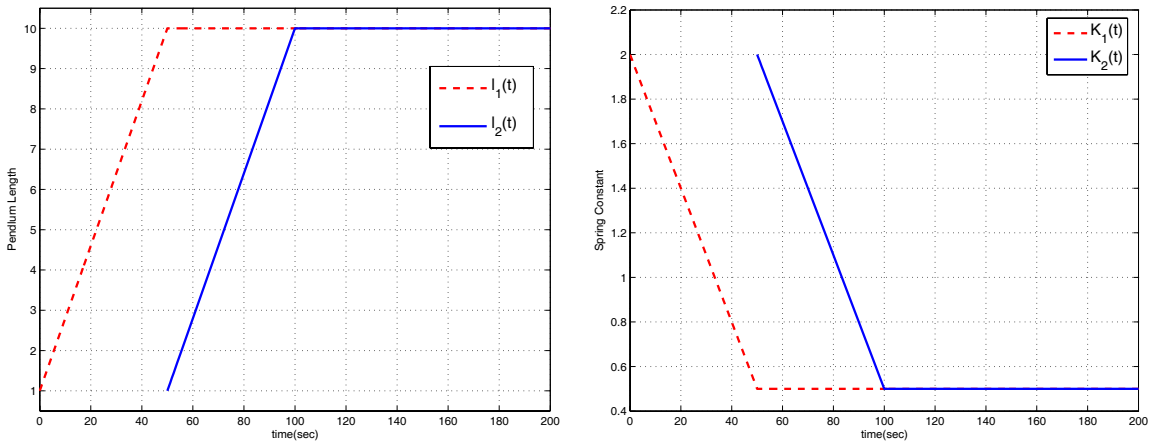

(a) Pendulum length (b) Torsional stiffness

Figure 6. Time-varying parameters

Figure 7 shows the time responses of θ_1 and θ_2 when no external disturbances are present. While the open-loop system exhibits large oscillations that are caused by restoring moment of torsional springs, the lead compensator in (16) (the Existing Controller) provides good regulation. When the lead compensator is augmented augmented as in Figure 5 ("EC with augmentation"), the transient response of θ_1 exhibits fast oscillations caused by initial adaptation of the NN weights. Thus adaptation is not desirable in a benign environment.

Figure 8 compares time responses of θ_1 and θ_2 when the structure is subject to the solar pressure torques $f_{s_1}(l_(t), \theta_1)$ and $\boldsymbol{f}_s(l_2(t), \boldsymbol{\theta})$ in (4) and (9). Since this is the environment in which the sailcraft operates, optimum positioning of the structure before it executes its mission is particularly important. Whereas the existing control system stabilizes the system with much longer settling time as shown in Figure 8, with the controller augmented, the time responses for θ_1 and θ_2 are almost the same as those in Figure 7 regardless of the solar torque disturbance. Figure 9 compares the command tracking performance of the controllers with and without augmentation. While the existing control system fails to regulate the system to the desired position, the augmented system drives the system into a desired set-point.

In general, a spacecraft is less influenced by gravity than are the vehicles on Earth. Nevertheless, atmospheric drag or solar radiation pressure for an orbiting spacecraft can lead to effects that are similar to the effect of gravity, and cause heavy particles to settle toward the front end of a moving spacecraft.[27] In other cases, direct gravitation effects, such as gravity gradient forces due to differences over an extended object, may be required to be taken into account when the spacecraft has a long and slender shape. In our example, when the pendulum evolves along the gravity vector, the gravitational force helps to stabilize the system into its equilibrium position. However, when the structure expands in a direction opposite to that of the gravity vector,the effect of gravity is destabilizing. In the next simulation, we introduce a reduced

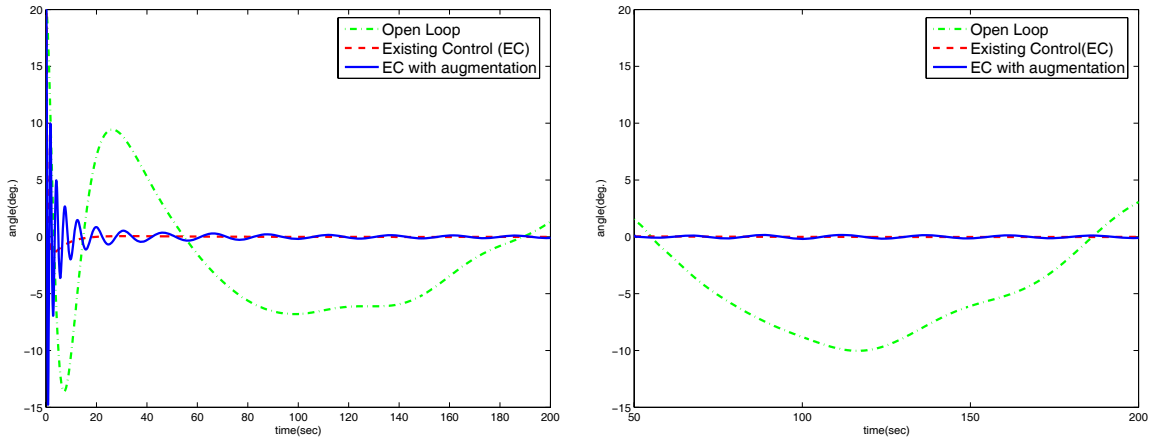

(a) θ_1 (b) θ_2

Figure 7. Evolution without any external disturbance

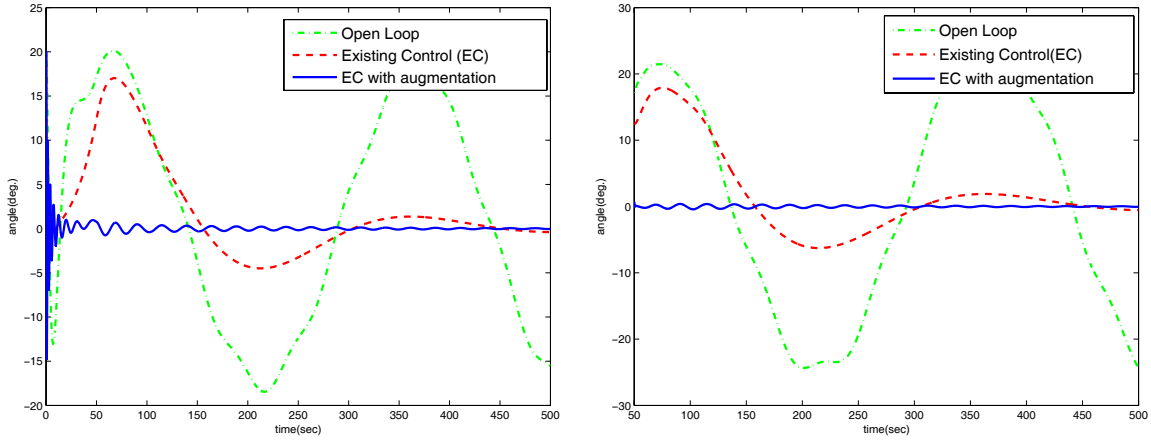

(a) θ_1 (b) θ_2

Figure 8. Evolution with the solar pressure

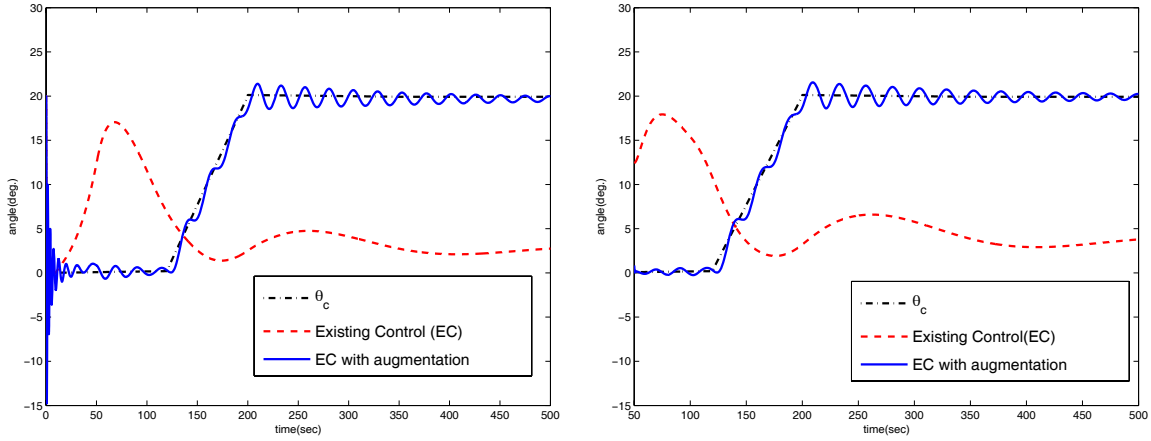

(a) θ_1 (b) θ_2

Figure 9. Tracking after evolution with the solar pressure

gravity $g_r = 0.98(m/s^2)$ that is 10% of the gravity on Earth

$$F_{a_x} = \begin{cases} -(m_1+m_2)g_r & \text{for} \quad 0 < t < t_1 \\ -m_1 g_r & \text{for} \quad t \geq t_1 \end{cases}, \; F_{b_x} = -m_2 g_r \text{ for } \quad t \geq t_1. \tag{44}$$

Figure 10 shows the time responses of θ_1 and θ_2 with these gravity terms present. Since the zero solution is an unstable equilibrium, the open-loop system goes immediately unstable, and the response for that case is not shown. In this case the lead compensator also fails, and the pendulum falls to a stable equilibrium state in which the masses are aligned with the gravity vector. The augmented controller manages to regulate the system to is unstable equilibrium state in which the masses are aligned in opposition to the gravity vector. While the lead compensator in (16) fails to restore the pendulum and falls into a stable equilibrium, the augmented controller still regulates the pendulum with respect to its unstable equilibrium. This case

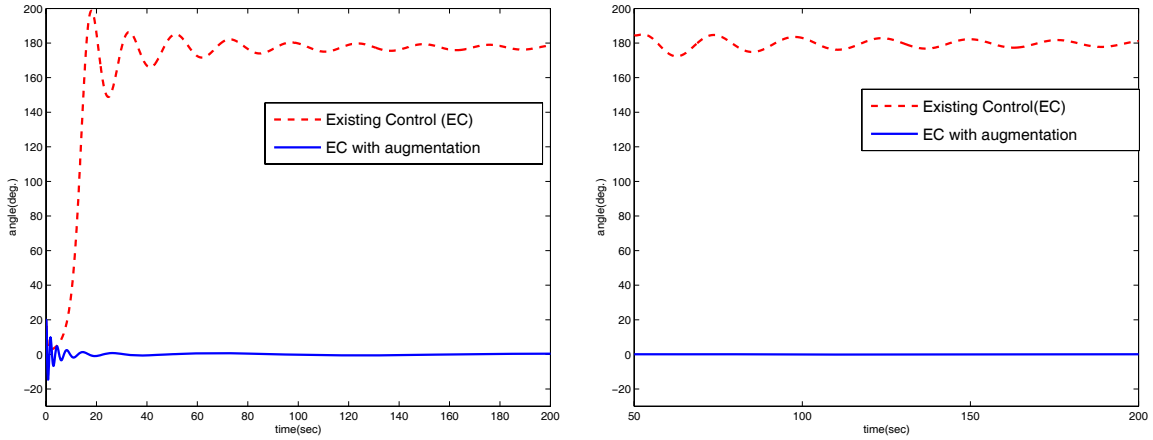

(a) θ_1 (b) θ_2

Figure 10. Time responses of the evolving pendulum with the 10% gravitational effect

is particularly interesting, because every fixed-gain decentralized controller design that was tried failed to regulate the pendulum to its unstable equilibrium condition when subjected to a gravity field. Figure 11 compares the time responses with the adaptive signal ("EC+$\nu_{dc} + \nu_{ad}$") to those without the adaptive signal ("EC+ν_{dc}"), and clearly indicates that stable behavior results from adaptive control. This is further

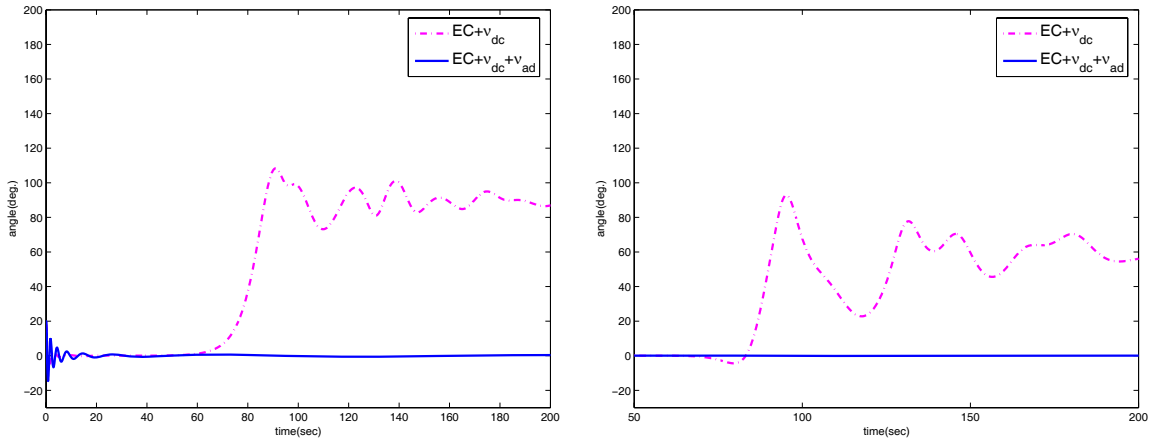

(a) θ_1 (b) θ_2

Figure 11. Time responses of the evolving pendulum with and without the adaptive signal ν_{ad} under the 10% gravitational effect

confirmed by comparing the modelling errors defined in (18), (19), and (20) to the adaptive signal $\nu_{i_{ad}}$, $i =$

1, 2, in (40). Figure 12 shows that the adaptive signals closely approximate for the time-varying modelling errors.

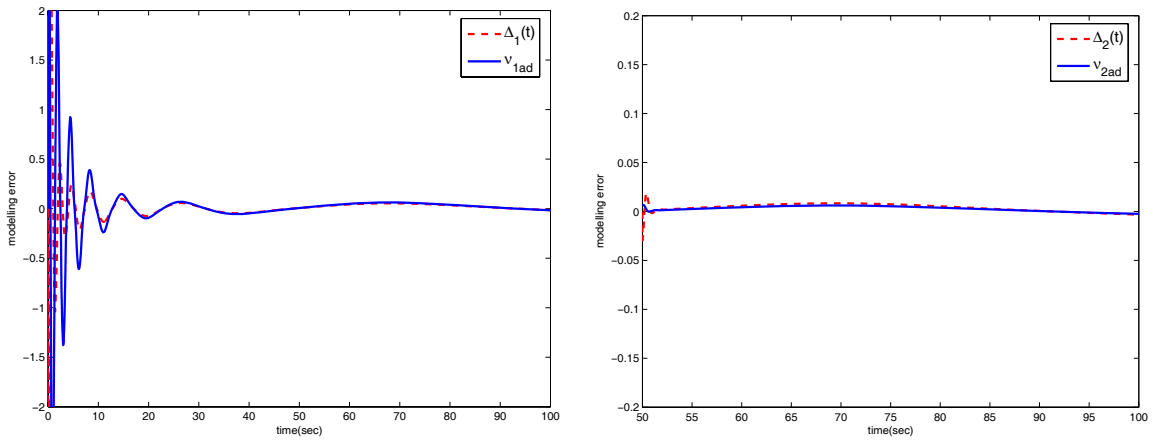

(a) θ_1 (b) θ_2

Figure 12. Modelling error and the adaptive signal with the gravitational effect

V. Conclusions and Future Research

We consider the feasibility of using neural network based adaptive control for evolving gossamer structure which is characterized by time-varying structural properties. A growing double pendulum is used to illustrate the control method. Nominal controllers are designed in a decentralized manner, and augmenting adaptive control elements are added. In a benign environment, the nominal controllers perform well, and successfully stabilize the evolving system. However, when solar radiation pressure or gravitational effects are introduced, the controllers augmented by the adaptive elements significantly outperform the nominal controllers.

To evaluate an adaptive method in a flexible solar sail boom, an experimental test is under way using the SAFE (Solar Array Flight Experiment) boom, which had previously been carried by Space shuttle and then has been set up for control structure interaction at NASA Marshall Space Flight Center. We hope to report in the near term the results of that experiment.

Acknowledgments

This research was supported by the NASA Marshall Space Flight Center, under grant number NAG8-1912.

References

[1]McInnes, C. R., *Solar Sailing: Technology, Dynamics, and Mission Applications*, Springer-Praxis Books in Astronautical Engineering, 2004.

[2]Murphy, D. and Wie, B., "Robust Thrust Control Authority for a Scalable Sailcraft," *14th AAS/AIAA Space Flight Mechanics Conference*, AAS 04-285, Maui,HI, 2004.

[3]Wie, B., "Dynamic Modeling and Attitude Control of Solar Sail Spacecraft: Part I," *Proceedings of AIAA guidance,navigation and control conference*, AIAA 2002-4572, Monterey, CA, 2002.

[4]Wie, B., "Dynamic Modeling and Attitude Control of Solar Sail Spacecraft: Part II," *Proceedings of AIAA guidance,navigation and control conference*, AIAA 2002-4573, Monterey, CA, 2002.

[5]Wie, B., "Solar Sail Attitude Control and Dynamics, Part 1," *AIAA Journal of Guidance, Control & Dynamics*, Vol. 27, No. 4, 2004.

[6]Rotunno, M., Basso, M., Pomè, A. B., and Sallusti, M., "A Comparison of Robust Attitude Control Techniques for a Solar Sail Spacecraft," *Proceedings of AIAA guidance,navigation and control conference*, AIAA 2005-6083, San Frrancisco, CA, 2005.

[7]Smith, S. W., Song, H., Baker, J. R., and Black, J., "Flexible Models for Solar Sail Control," *46th AIAA/ASME/ASCE/AHS/ASC Structures, Structural Dynamics and Materials Conference*, AIAA 2005-1801, Austin, TX, 2005.

[8]Graybeal, N. and Craig, J. I., "Deployment Modeling of Solar Sail Structures," *Proceedings of AIAA guidance,navigation and control conference*, AIAA-2006-6336, Keystone, CO, August 2006.

[9]Sleight, D. W., Michii, Y., Lichodziejewski, D., and Derbès, B., "Structural Analysis of an Inflation-deployed Solar Sail with Experimental Validation," *41st AIAA/ASME/SAE/ASEE Joing Propulsion Conference*, AIAA 2005-3727, Tucson, AZ, 2005.

[10]Marino, R. and Tomei, P., *Nonlinear Control Design: Geometric, Adaptive, & Robust*, Prentice Hall, New Jersey, 1995.

[11]Ioannou, P. and Sun, J., *Robust Adaptive Control*, Prentice-Hall, Englewood Cliffs, NJ, 1996.

[12]Hovakimyan, N., Lavretsky, E., Yang, B.-J., and Calise, A., "Coordinated Decentralized Adaptive Output Feedback for Control of Interconnected Systems," *IEEE Transactions on Neural Networks*, Vol. 16, No. 1, 2005, pp. 185–194.

[13]Kutay, A. T., Fowler, J. M., Calise, A. J., and D'Andrea, R., "Distributed Adaptive Output Feedback Control Design and Application to a Formation Flight Experiment," *Proceedings of AIAA guidance,navigation and control conference*, Aug. 2005.

[14]Hornik, N., Stinchcombe, M., and White, H., "Multilayer feedforward networks are universal approximators," *Neural Networks*, Vol. 2, 1989, pp. 359–366.

[15]Ge, S., Lee, T., and Harris, C., *Adaptive Neural Network Control of Robotic Manipulators*, World Scientific, 1998.

[16]Lewis, F., Jagannathan, S., and Yeşildirek, A., *Neural Network Control of Robot Manipulators and Nonlinear Systems*, Taylor & Francis, 1999.

[17]Spooner, J. T., Maggiore, M., Ordóñez, R., and Passino, K. M., *Stable Adaptive Control and Estimation for Nonlinear Systems- Neural and Fuzzy Approximator Techniques*, John Wiley & Sons, New York, NY, 2002.

[18]Lavretsky, E., Hovakimyan, N., and Calise, A., "Upper Bounds for Approximation of Continuous-Time Dynamics Using Delayed Outputs and Feedforward Neural Networks," *IEEE Transactions on Automatic Control*, Vol. 48, No. 9, 2003, pp. 1606–1610.

[19]Kim, N., Calise, A. J., Hovakimyan, N., Prasad, J., and Corban, J. E., "Adaptive Output Feedback for High-Bandwidth Flight Control," *AIAA Journal of Guidance, Control & Dynamics*, Vol. 25, No. 6, 2002, pp. 993–1002.

[20]Calise, A., Yang, B.-J., and Craig, J., "An Augmenting Adaptive Approach to Control of Flexible Systems," *AIAA Journal of Guidance, Control & Dynamics*, Vol. 27, No. 3, 2004, pp. 387–396.

[21]Yang, B.-J., Hovakimyan, N., Calise, A., and Craig, J., "Experimental Validation of an Augmenting Approach to Adaptive Control of Uncertain Nonlinear Systems," *Proceedings of AIAA guidance,navigation and control conference*, AIAA-2003-5715, Austin, TX, 2003.

[22]Yang, B.-J., Calise, A., and Craig, J., "Adaptive Output Feedback Control of a Flexible Base Manipulator," *Proceedings of AIAA guidance,navigation and control conference*, AIAA-2004-5322, Providence, RI, August 2004.

[23]Hovakimyan, N., Yang, B.-J., and Calise, A. J., "Adaptive Output Feedback Control Methodology Applicable to Non-Minimum Phase Nonlinear Systems," *Automatica*, Vol. 42, No. 4, April 2006, pp. 513–522.

[24]Hovakimyan, N., Yang, B.-J., and Calise, A., "An Adaptive Output Feedback Control Methodology for Non-Minimum Phase Systems," *Proceedings of Conference on Decision and Control*, Las Vegas, NV, 2002, pp. 949–954.

[25]Calise, A., Hovakimyan, N., and Idan, M., "Adaptive Output Feedback Control of Nonlinear Systems using Neural Networks," *Automatica*, Vol. 37, No. 8, 2001, pp. 1201–1211.

[26]Hovakimyan, N., Nardi, F., Kim, N., and Calise, A., "Adaptive Output Feedback Control of Uncertain Systems using Single Hidden Layer Neural Networks," *IEEE Transactions on Neural Networks*, Vol. 13, No. 6, 2002.

[27]Gorney, D., Blake, J., Koons, H., Schulz, M., Vampola, A., and Walterscheid, R., "The Space Environment and Survivability," *Space Mission Analysis and Design*, edited by W. J. Larson and J. R. Wertz, Microcosm, Inc. and Kluwer Academic Publishers, 2nd ed., 1992.